

Dynamic Input Mapping Inversion for Algebraic Loop-Free Control in Hydraulic Actuators

Alessio Dallabona, Patrik Schermann, Mogens Blanke, Dimitrios Papageorgiou

Abstract—The application of nonlinear control schemes to electro-hydraulic actuators often requires several alterations in the design of the controllers during their implementation. This is to overcome the challenges that frequently arise from the inherent complexity of such control algorithms owing to model nonlinearities. Moreover, advanced control solutions for this type of systems often introduce input algebraic loops and chatter, which considerably degrade the tracking performance. This study presents a nonlinear control architecture for hydraulic actuators that comprises low-complexity modules, based on well-established designs that facilitate robust high performance in tracking without introducing the aforementioned limitations. Specifically, the proposed solution consists of two variants of a position controller for the hydraulic cylinder and a dynamic input-mapping inversion module to avoid algebraic loops in the control input. The stability of the closed-loop system is analysed using arguments from Lyapunov theory for cascaded non-autonomous nonlinear systems. The effectiveness of the proposed solution is evaluated on a high-fidelity simulator of a wind turbine pitch system. Appropriate quantitative metrics are finally defined to evaluate the closed-loop system performance in comparison to state-of-the-art nonlinear design.

Index Terms—electro-hydraulic actuator, nonlinear control, parameter estimation, mapping inversion

I. INTRODUCTION

ELECTRO-HYDRUALIC actuators (EHA) are commonly used in industrial applications because of their high power density and resilience to harsh environment. Typical applications include aviation, manufacturing, marine/offshore engineering, robotics and energy systems [1]–[3].

Although Proportional-Integral-Differential (PID) controllers constitute the industrial standard in these application domains, they often fall short in maintaining high performance in the presence of strong nonlinearities and uncertainties that characterize hydraulic actuator systems. This has motivated the exploration of nonlinear control alternatives that can improve performance and enhance closed-loop robustness over the entire envelope of operation. The complexity, however, of system dynamics often hinders effective application of nonlinear model-based solutions such as feedback linearization (FL) or sliding mode control (SMC) because several limiting assumptions and modelling simplifications need be imposed to apply these methods.

A common heavy simplification concerns the valve dynamics, where two main issues can be identified. A first limitation

is encountered when a system model cannot be written as an affine form $\dot{x} = f(x) + g(x)u$, as the vector field of a valve depends non-linearly on the input. A common approach to address this issue is to use the input value at the previous time instant, under the assumption that the input u is slowly varying. This removes the nonlinearity and avoids the introduction of an algebraic loop, at the cost of increased chatter in the control signal [4]. The second design challenge arises with inclusion of actuator dynamics, which increase the relative degree of the system, thus making the design much more complicated, as will be discussed later. Neglecting the valve dynamics during the design stage can simplify implementation but may potentially result in a quite demanding control action going beyond obtainable valve response. This may introduce additional chatter and potential wind up effects.

Furthermore, micro-movements in EHAs are responsible for local heating of hydraulic oil, which degrades oil quality. This leads to increased friction, and eventually to wear and potential damage of a valve [5]. It is therefore essential to establish control designs that combine the performance and robustness features of nonlinear solutions, but avoid excessive actuation demand.

Several studies in the existing literature have reported solutions that adopt nonlinear strategies for controlling hydraulic systems. A cascaded feedback linearization controller with a sliding mode observer was designed in [6]. Sliding mode was explored in a standard fashion in [7], in combination with adaptive control in [8], with an integral sliding surface in [9] and later in [10] to eliminate the velocity state in the control action. Adaptive solutions have been applied by means of backstepping, in e.g. [11], [12], [13], and [14]. The authors in [15] used a coordinate transformation and tuning functions to obtain a backstepping controller that included the valve dynamics. The high relative degree led to a complex solution. Except for the latter, all the other solution adopted the strategy presented in [4] to cancel the algebraic loop, and do not account for the valve dynamics in the design of the controller.

The aim of this paper is to leverage the results on online estimation of nonlinearly parametrised perturbations [16], [17] as a dynamical mapping inversion (MI) algorithm to derive the control input from a virtual input designed via classical nonlinear methods. The paper shows how a modular and straightforward design is achieved, and how the MI can reconstruct the control signal without introducing algebraic loops. Moreover, it is shown how the suggested approach facilitates a systematic commissioning feature, namely, how it can accommodate valve specification parameters such that

Manuscript received October 29, 2024; revised December 31, 2024. (Corresponding author: Alessio Dallabona.)

All the authors are with Technical University of Denmark (DTU), 2800, Kgs. Lyngby, Denmark (email: aldall@dtu.dk; s212374@student.dtu.dk; mobil@dtu.dk; dimpa@dtu.dk)

only frequencies that can actually be delivered by the valve are allowed in the control input. In this way, the performance can be improved and chatter in the input be significantly reduced.

This article contributes by

- 1) presenting a modular architecture for nonlinear control of hydraulic actuators without introducing algebraic loops or limiting assumptions on the input signal,
- 2) proposing a scheme for reconstructing the control signal by leveraging a nonlinear parameter estimation algorithm for dynamically inverting the mapping between control input and virtual input,
- 3) introducing a systematic method to tune the dynamical mapping inversion component according to the actuator parameters,
- 4) providing rigorous stability and boundedness analyses of the closed-loop dynamics under different control laws,
- 5) demonstrating the effectiveness of the proposed solution against conventional nonlinear control methods for industrial EHA systems in a real case scenario, using a high-fidelity simulator.

The remainder of the paper is organized as follows. Sec. II presents the hydraulic actuator system and defines the problem at hand. Sec. III designs controllers following commonly accepted standards, and Sec. IV proposes a new algorithm and presents features and benefits in contrast to the standard existing approaches. Stability of the closed-loop system is the subject of Sec. V. Sec. VI presents a case study of a wind turbine pitch control, and results from high fidelity simulation are shown in Sec. VII. Finally, conclusions and future directions are staged in Sec. VIII.

II. PROBLEM DEFINITION

An electro-hydraulic actuator is composed of an hydraulic cylinder driven by a directional control valve, as shown in Fig. 1. The pressures p_p and p_r in the piston-side and rod-side chambers of the cylinder are varied according to the valve spool position x_v . This allows for control of both position and velocity (x_c and v_c) of the the cylinder's piston. The model for a generic electro-hydraulic actuator is given by [9]:

$$\begin{aligned}
 M\dot{v}_c &= A_p p_p - A_r p_r - F_{fr} - F_{ext} \\
 \dot{x}_c &= v_c \\
 \dot{p}_p &= \frac{B_{e,p}(p_p)}{V_p(x_c)} [Q_p(x_v) - A_p v_c] \\
 \dot{p}_r &= \frac{B_{e,r}(p_r)}{V_r(x_c)} [-Q_r(x_v) + A_r v_c] \\
 \dot{v}_v + 2\xi\omega_0 v_v + \omega_0^2 x_v &= \omega_0^2 u_x \\
 \dot{x}_v &= v_v,
 \end{aligned} \tag{1}$$

where M is the piston mass, A_p and A_r the cylinder cross sections in the two chambers, F_{fr} and F_{ext} the friction force and the external load respectively, and $B_{e,i}(p_i)$ the effective bulk modulus of the oil in the i -th component. The control input u_x is a position reference for the control valve's spool. The terms

$$\begin{aligned}
 V_p(x_c) &= V_{0,p} + A_p x_c \\
 V_r(x_v) &= V_{0,r} + A_r (x_{c,m} - x_c).
 \end{aligned} \tag{2}$$

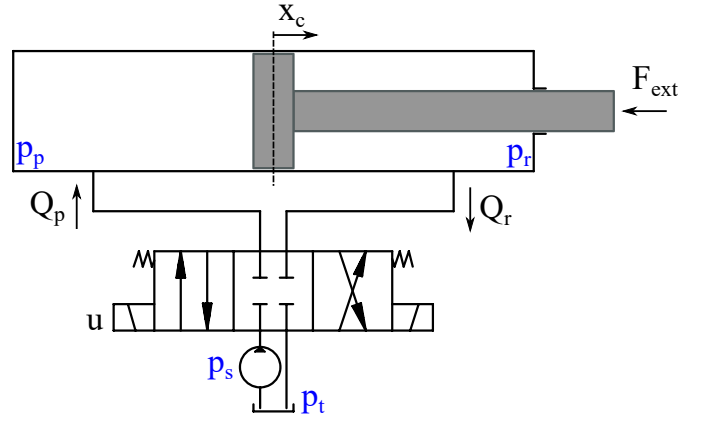


Fig. 1. Generic electro-hydraulic actuator configuration: above, the linear cylinder with piston and rod; below, the flow control valve, oil pump and drain.

represent the volumes of the cylinder chambers.

The flows are calculated as

$$\begin{aligned}
 Q_p(x_v) &= K(x_v) \sqrt{\Delta_{pp}(x_v)} \\
 Q_r(x_v) &= K(x_v) \sqrt{\Delta_{pr}(x_v)}.
 \end{aligned} \tag{3}$$

where the nonlinear function $K(x_v)$ determine the valve flow coefficient based on its spool position, and

$$\begin{aligned}
 \Delta_{pp} &= (p_s - p_p) H(x_v) + (p_p - p_t) H(-x_v) \\
 \Delta_{pr} &= (p_r - p_t) H(x_v) + (p_s - p_r) H(-x_v),
 \end{aligned} \tag{4}$$

with $H(\cdot)$ being the Heaviside step function.

The control objective in EHA systems is the tracking of a reference signal for the cylinder piston position x_c . By inspecting the cylinder position dynamics in Eq. 1 it is easily seen that the system corresponding to the position error defined as

$$e \triangleq x_c - r, \tag{5}$$

has relative degree 5, i.e. e needs to be differentiated five times in order to arrive to a controller canonical form

$$e^{(\alpha)} = f(u), \tag{6}$$

which is suitable for control design.

For the class of EHA systems this introduces a high degree of complexity due to the strong nonlinear couplings between the various pressure terms. A common approach adopted in the literature to alleviate this complexity is the introduction of a simplifying assumption, namely the neglect of the valve dynamics. This implies that the position x_v inside the terms $Q_p(x_v)$ and $Q_r(x_v)$ can instantaneously assume any desired value and is, therefore, considered the effective control input for the system, i.e. $u \triangleq x_v$, with $u \in [-1, 1]$.

An additional frequent simplification made in many reported studies is considering one single constant value for the bulk modulus of the oil for both chambers, i.e., $B_{e,p} = B_{e,r} = B > 0$. The resulting model, which is most commonly used in the industry for control design, is [18]:

$$\begin{aligned}
M\dot{v}_c &= A_p p_p - A_r p_r - F_{Fr} - F_{ext} \\
\dot{x}_c &= v_c \\
\dot{F}_h &= A_p \dot{p}_p - A_r \dot{p}_r \\
&= \frac{A_p B}{V_p(x_c)} [Q_p(u) - A_p v_c] - \frac{A_r B}{V_r(x_c)} [A_r v_c - Q_r(u)],
\end{aligned} \tag{7}$$

where the hydraulic force $F_h = A_p p_p - A_r p_r$ is introduced to avoid considering internal dynamics.

III. BASELINE NONLINEAR CONTROL DESIGN

Considering the model presented in Eq. 7 and the position error e defined in Eq. 5, the dynamics constitutes a relative degree 3 system and reads:

$$\begin{aligned}
e^{(3)} &= -\frac{\dot{F}_{fric} + \dot{F}_{ext}}{M} - \frac{A_p^2 B}{M V_p} v_c - \frac{A_r^2 B}{M V_r} v_c - r^{(3)} + \\
&\quad \frac{A_p B}{M V_p} Q_p(u) + \frac{A_r B}{M V_r} Q_r(u) \triangleq \varpi_{FL}.
\end{aligned} \tag{8}$$

Intermediate derivatives are given by

$$\begin{aligned}
\dot{e} &= v_c - \dot{r} \\
\ddot{e} &= -\frac{F_{fric} + F_{ext}}{M} + \frac{A_p p_p - A_r p_r}{M} - \ddot{r},
\end{aligned} \tag{9}$$

where the virtual input $\varpi_{FL} = \varpi_{FL}(t, \mathbf{x}, u)$ is a function of time, of states $\mathbf{x} \triangleq [v_c \ x_c \ F_h]^T$, and of the control input u .

Two basic control solutions are first presented to demonstrate both the effectiveness and the reasons behind the development of a new algorithm. Feedback linearization is presented as a baseline nonlinear control design, which is popular for adaptive nonlinear control solutions. A supertwisting sliding mode control design is shown as a second popular solution.

A. Feedback linearization (FL)

A FL controller is obtained from writing the error derivative dynamics as follows,

$$\dot{\mathbf{e}} = \underbrace{\begin{bmatrix} 0 & 1 & 0 \\ 0 & 0 & 1 \\ 0 & 0 & 0 \end{bmatrix}}_{\mathbf{A}_{FL}} \underbrace{\begin{bmatrix} e \\ \dot{e} \\ \ddot{e} \end{bmatrix}}_{\mathbf{e}} + \underbrace{\begin{bmatrix} 0 \\ 0 \\ 1 \end{bmatrix}}_{\mathbf{B}_{FL}} \varpi_{FL}. \tag{10}$$

Selecting

$$\varpi_{FL} = -\mathbf{K}_{FL} \mathbf{e} \tag{11}$$

with \mathbf{K}_{FL} obtained with a standard linear design (eigvalue assignment, LQR, etc.), renders the closed-loop system globally exponentially stable (GES) with the rate of decay being defined by the gain \mathbf{K}_{FL} . The related control input u is isolated from Eq. 11 taking also Eq. 8, and Eq. 9 into account.

B. Supertwisting SMC

Sliding mode controllers aim at enforcing the trajectories $e(t) \in \mathbb{R}^3$ of the error system onto a pre-designed manifold $\mathcal{S} = \{e \in \mathbb{R}^3 \mid s(e) = 0\}$. The variable s is referred to as the *sliding variable* and is designed to guarantee exponential stability of the error system, so long s is regulated at the origin.

In order to leverage the reduced chatter properties of the well-studied supertwisting sliding mode control designs [19], the dynamics of s should be brought into the form of Eq. 6 with a single differentiation. Therefore, the sliding variable s is defined as:

$$s = \ddot{e} + \lambda_2 \dot{e} + \lambda_1 e, \tag{12}$$

where λ_1, λ_2 are selected such that the characteristic polynomial in Eq. 12 is Hurwitz. The dynamics of the sliding variable s is:

$$\dot{s} = \underbrace{e^{(3)} + \lambda_2 \ddot{e} + \lambda_1 \dot{e}}_{\varpi_{ST}(t, \mathbf{x}, u)}, \tag{13}$$

where the right-hand side is of Eq. 13 is again a function ϖ_{ST} of time, the states and the control input u . Eq. 12 implies global exponential stability for the origin of the piston position error when the system is in sliding mode, i.e. when $s = \dot{s} = 0$. This can be achieved by selecting

$$\varpi_{ST} = -k_1 [s]^{1/2} - k_2 \int_0^t \text{sgn}(s(\tau)) d\tau, \tag{14}$$

where $k_1, k_2 > 0$. Similar to the controller case in the previous subsection, the control input is derived by isolating the term u in equation 14.

C. Control input

The final step for designing the controllers is deriving the control input u for which the closed-loop system dynamics is shaped, via the previously presented design methods. From Eq. 8 it is noticed that the error dynamics depends on the terms F_{ext} and F_{fr} , and their derivatives. Such terms are in general unknown and need be estimated to compute the control input u .

1) *Disturbance observer*: Although dedicated tests can be run to identify the friction coefficients, it is convenient in this investigation to assume the friction term to be unknown. This allows for lumping it together with the external load in a single term $F_d = F_{ext} + F_{fr}$, which can then be estimated with a conventional linear observer. Such an observer can be designed based on the measured pressures as follows,

$$\dot{\hat{z}} = \underbrace{\begin{bmatrix} 0 & -\frac{1}{M} \\ 0 & 0 \end{bmatrix}}_{\mathbf{A}} \hat{z} + \underbrace{\begin{bmatrix} A_p p_p - A_r p_r \\ M \\ 0 \end{bmatrix}}_{\mathbf{L}} + \underbrace{\begin{bmatrix} L_1 \\ L_2 \end{bmatrix}}_{\mathbf{L}} \underbrace{\begin{bmatrix} 1 & 0 \end{bmatrix}}_{\mathbf{C}} \hat{z}, \tag{15}$$

where $\hat{z} = [\hat{v}_c \ \hat{F}_d]^T$, $\tilde{z} \triangleq z - \hat{z}$ and \mathbf{L} chosen such that $\mathbf{A} - \mathbf{L}\mathbf{C}$ is Hurwitz, ensuring that the disturbance term F_d can be reconstructed with a bounded error [20]. Furthermore, since $z \in \mathcal{L}_\infty$ and $\mathbf{A} - \mathbf{L}\mathbf{C}$ is Hurwitz by design, it holds that

$$\|\tilde{z}\| = \|(\mathbf{A} - \mathbf{L}\mathbf{C}) \tilde{z}\| \leq -\lambda_{\min}(\mathbf{A} - \mathbf{L}\mathbf{C}) \|\tilde{z}\|_\infty \triangleq L_z, \tag{16}$$

where L_z is a positive real number. Thus, \dot{F}_d is also reconstructed with a bounded error. Global asymptotic stability of the entire closed-loop system will be proved subsequently.

2) *Control input derivation*: Directly isolating u in Eq. 11 and Eq. 13 is not possible: while it may be possible to invert the $K(u)$ function in Eq. 3, the control input also appears inside the Heaviside functions, generating an algebraic loop where the derived input depends on the input itself. The standard way to solve the problem is the one described in [4]:

$$\begin{aligned} Q_p(t, u) &= K(u) [\sqrt{p_s - p_p} H(u) + \sqrt{p_p - p_t} H(-u)] \\ &\approx Ku [\sqrt{p_s - p_p} H(u_{-1}) + \sqrt{p_p - p_t} H(-u_{-1})] \\ &= K_{Qp} u, \end{aligned} \quad (17)$$

$$\begin{aligned} Q_r(t, u) &= K(u) [\sqrt{p_r - p_t} H(u) + \sqrt{p_s - p_r} H(-u)] \\ &\approx Ku [\sqrt{p_r - p_t} H(u_{-1}) + \sqrt{p_s - p_r} H(-u_{-1})] \\ &= K_{Qr} u, \end{aligned} \quad (18)$$

where the term u_{-1} represents the value of the input at the previous time step. In this way, the algebraic loop is eliminated and u enters linearly in both equations. By defining

$$g = \frac{A_p B}{MV_p} K_{Qp} + \frac{A_r B}{MV_r} K_{Qr}, \quad (19)$$

the standard feedback linearization controller is then,

$$u_{FL} = \frac{1}{g} \left[\frac{\dot{F}_d}{M} + \frac{A_p^2 B}{MV_p} v_c + \frac{A_r^2 B}{MV_r} v_c + r^{(3)} - K_{FL} \underline{e} \right], \quad (20)$$

and the standard super-twisting sliding mode controller is,

$$\begin{aligned} u_{ST} &= \frac{1}{g} \left[\frac{\dot{F}_d}{M} + \frac{A_p^2 B}{MV_p} v_c + \frac{A_r^2 B}{MV_r} v_c - \lambda_2 \ddot{e} - \lambda_1 \dot{e} \right. \\ &\quad \left. + r^{(3)} - k_1 |s|^{1/2} - k_2 \int_0^t \text{sgn}(s) d\tau \right]. \end{aligned} \quad (21)$$

The $K(u)$ linearization is then reflected into uncertainties in the input term g and in the terms K_{Qp} and K_{Qr} .

IV. CASCADED CONTROL DESIGN

The delay operator introduced to avoid the formation of algebraic loops simplified the controller implementation with the drawback of increasing unwanted chatter on the control signal, with the consequences on oil quality described above. The solution proposed in this article for avoiding this, is to leverage a virtual input for the controller design and dynamically deriving a real input that produces the virtual one required by the controller. The block diagram is shown in Fig. 2.

By defining a virtual input as

$$v \triangleq \frac{A_p B}{MV_p} Q_p(u) + \frac{A_r B}{MV_r} Q_r(u), \quad (22)$$

Eq. 8 can be rewritten as

$$e^{(3)} = -\frac{\dot{F}_{fric} + \dot{F}_{ext}}{M} - \frac{A_p^2 B}{MV_p} v_c - \frac{A_r^2 B}{MV_r} v_c - r^{(3)} + v, \quad (23)$$

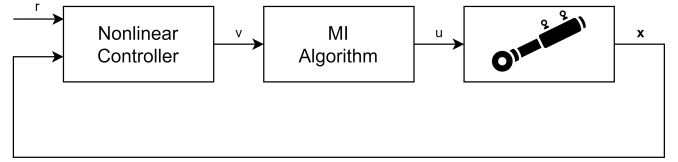


Fig. 2. Block diagram of the proposed algorithm: Cascaded control with dynamic input mapping inversion.

where the virtual input v is a function of time and the control input u , and is now present as a linear term. The feedback linearizing and supertwisting control designs are now defined in terms of the associated virtual inputs as, respectively,

$$v_{FL} = \frac{\dot{F}_d}{M} + \frac{A_p^2 B}{MV_p} v_c + \frac{A_r^2 B}{MV_r} v_c + r^{(3)} - K_{FL} \underline{e}, \quad (24)$$

and

$$\begin{aligned} v_{ST} &= \frac{\dot{F}_d}{M} + \frac{A_p^2 B}{MV_p} v_c + \frac{A_r^2 B}{MV_r} v_c - \lambda_2 \ddot{e} - \lambda_1 \dot{e} \\ &\quad + r^{(3)} - k_1 |s|^{1/2} - k_2 \int_0^t \text{sgn}(s(\tau)) d\tau. \end{aligned} \quad (25)$$

A. Dynamic mapping inversion algorithm

The last part of the proposed method constitutes the derivation of the control input u by solving Eq. 22 for u in each case. A dynamic nonlinear mapping inversion scheme is adopted from [16] for this purpose, allowing for re-formulating of the input calculation into a parameter estimation problem in u for a nonlinearly parametrized regressor.

Specifically, let $\rho : [0, \infty) \times \mathbb{R}^3 \times [-1, 1] \rightarrow \mathbb{R}$ with

$$\rho(t, \mathbf{x}, u) = \frac{A_p B}{MV_p} Q_p(t, \mathbf{x}, u) + \frac{A_r B}{MV_r} Q_r(t, \mathbf{x}, u) \quad (26)$$

be a mapping from any given actual control input u to the virtual input that was earlier defined in Eq. 22. Assume that for every value v at each time instant there exists an appropriate value of the control input u^* such that $v = \rho(u^*)$. It has been shown [16], [17] that the estimation law

$$\dot{u} = \gamma \mu(t, \mathbf{x}, u) (v - \rho(t, \mathbf{x}, u)), \quad (27)$$

where $\gamma > 0$ is a tuning gain and $\mu(t, \mathbf{x}, u)$ a function to be designed, ensures exponential convergence of the estimation error $\tilde{u} \triangleq u^* - u$ to the origin if the following conditions hold for all pairs (u^*, u) :

Condition 1. There exists a positive definite real function $\sigma(t, \mathbf{x})$ such that

$$\mu(t, \mathbf{x}, u^*) \left. \frac{\partial \rho}{\partial u} \right|_u + \left. \frac{\partial \rho}{\partial u} \right|_{u^*} \mu(t, \mathbf{x}, u) \geq 2\sigma(t, \mathbf{x}). \quad (28)$$

Condition 2. There exists a positive real number $L_\mu > 0$ such that

$$|\rho(t, \mathbf{x}, u^*) - \rho(t, \mathbf{x}, u)| \leq L_\mu |\tilde{u}| \sqrt{\sigma(t, \mathbf{x})}. \quad (29)$$

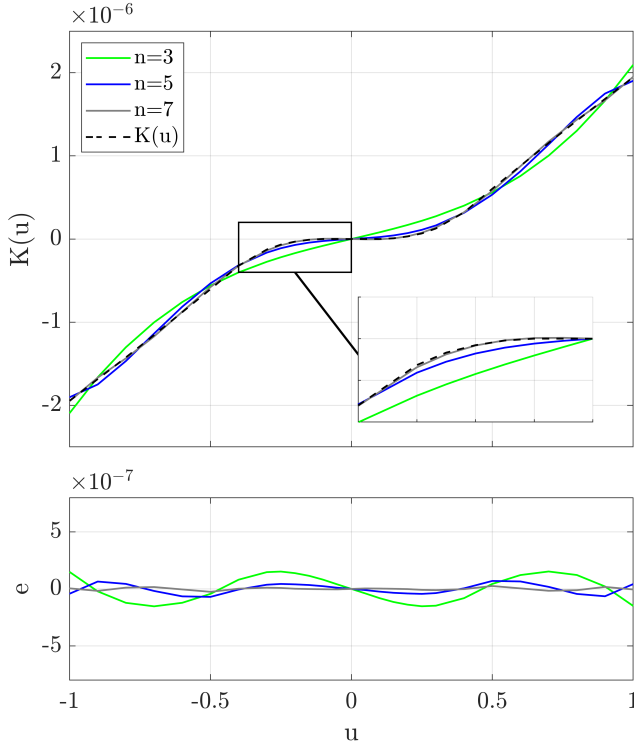


Fig. 3. Lookup table approximation with polynomial functions.

Condition 3 (Persistency of excitation). There exist positive constants $T, \alpha_0 > 0$ such that

$$\int_t^{t+T} \sigma(\tau, \mathbf{x}(\tau)) d\tau \geq \alpha_0 \mathbf{I}, \quad (30)$$

where \mathbf{I} is the identity matrix.

Remark 1. If the mapping ρ is not injective, then under Conditions 1-3, the estimation law in Eq. 27 will ensure that u converges to an appropriate value such that $\rho(t, u)$ converges to v exponentially fast.

A typical choice for μ is the gradient of ρ with respect to u . However, computation of μ requires differentiation of the nonlinear function $K(u)$ present in Eq. 3 and, since the latter is usually available as a lookup table, it is approximated by an appropriate polynomial function of u . Fig. 4 illustrates an example of different polynomial approximations for $K(u)$, i.e.

$$K(u) = \sum_{i=0}^n \alpha_i u^i, \quad (31)$$

with a fifth-order polynomial yielding the best fit.

This particular approximation also ensures that $\frac{\partial K}{\partial u} > 0, \forall u \in [-1, 1]$ as shown in Fig. 4, which will be useful later in proving the validity of the convergence conditions. The function of μ can now be selected as

$$\mu(t, \mathbf{x}, u) \triangleq \frac{\partial K}{\partial u} \left(\frac{A_p B}{M V_p} \sqrt{\Delta_{pp}(u)} + \frac{A_r B}{M V_r} \sqrt{\Delta_{pr}(u)} \right) > 0, \quad (32)$$

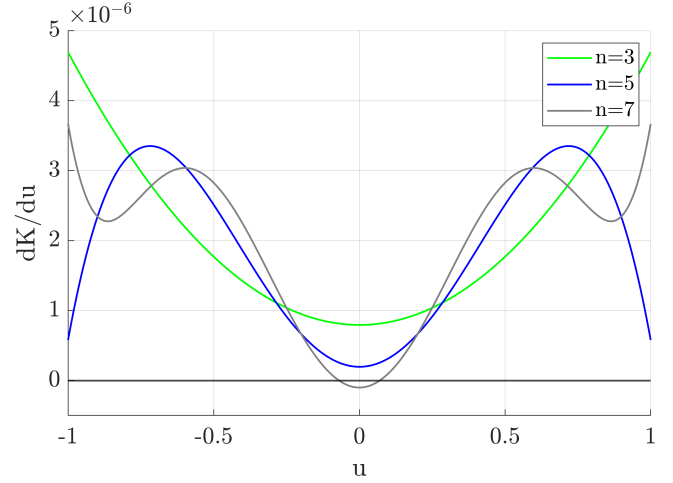


Fig. 4. Verification of derivative for algorithm convergence condition.

since the quantity in the parenthesis is always positive. Evaluation of Condition 1 leads to

$$\begin{aligned} \mu(t, \mathbf{x}, u^*) \frac{\partial \rho}{\partial u} \Big|_{u^*} + \mu(t, \mathbf{x}, u) \frac{\partial \rho}{\partial u} \Big|_{u^*} &= 2\mu(t, \mathbf{x}, u^*) \mu(t, \mathbf{x}, u) \\ &\geq 2 \left(\inf_u \mu(t, \mathbf{x}, u) \right)^2 \triangleq \sigma(t, \mathbf{x}) > 0. \end{aligned} \quad (33)$$

Moreover, since $\frac{\partial \rho}{\partial u}$ is bounded, there exists a Lipschitz constant $L_u > 0$ such that

$$|\rho(t, \mathbf{x}, u^*) - \rho(t, \mathbf{x}, u)| < L_u |\tilde{u}| \leq \frac{L_u |\tilde{u}| \sqrt{\sigma(t, \mathbf{x})}}{\sqrt{\inf_{(t, \mathbf{x})} \sigma(t, \mathbf{x})}} \quad (34)$$

which fulfills Conditions 1,2 with

$$L_\mu = \frac{L_u}{\sqrt{\inf_{(t, \mathbf{x})} \sigma(t, \mathbf{x})}}.$$

Finally, Condition 3 is satisfied by the definition of σ since $\sigma(t, \mathbf{x}) > 0, \forall (t, \mathbf{x}) \in \mathbb{R}_{\geq 0} \times \mathbb{R}^3$.

Remark 2. The μ function that was chosen for the purpose is an approximation of the gradient, where the dependency on u in the terms Δ_{pp} and Δ_{pr} is neglected during differentiation, since it only appears inside a Heaviside function. Hence, it would only be reflected in additional spikes in case a discontinuity is present during switching.

V. STABILITY ANALYSIS

The stability of the closed-loop system is analyzed by including the nonlinear controller, the dynamical mapping inversion, and the disturbance estimator. By writing it in the form of a feedback interconnected system

$$\begin{aligned} \Sigma_1 : \dot{\zeta} &= \mathbf{f}_1(\zeta, \tilde{u}) \\ \Sigma_2 : \dot{\tilde{u}} &= \mathbf{f}_2(\zeta, \tilde{u}) \end{aligned} \quad (35)$$

and by fulfilling the following conditions:

Condition 4. Unperturbed Σ_1 ($\tilde{u} = 0$) is Uniformly GES

Condition 5. Solutions of Σ_2 are Uniformly Ultimately Bounded (UUB)

Condition 6. $\forall(t, \zeta) \in [0, \infty) \times \mathbf{R}^2$

$$\frac{\partial V(t, \zeta)}{\partial \zeta} h(t, \tilde{u}) = o(W(\zeta)), \quad (36)$$

the overall closed-loop system is globally UUB according to Theorem 1 from [21].

Let $v^* = \rho(u^*)$ be the required virtual controller and u^* the related control input, one can define

$$\tilde{v} \triangleq v^* - v = \rho(u^*) - \rho(u), \quad (37)$$

for some arbitrary u and v , with $\tilde{u} = u^* - u$ having been defined earlier. The two closed-loop systems obtained by closing the loop with the FL controller and the ST-SMC controller are, respectively:

$$\begin{aligned} \Sigma_{1,FL} : \dot{\mathbf{e}} &= (\mathbf{A}_{FL} - \mathbf{B}_{FL}K_{fl}) \mathbf{e} + \boldsymbol{\xi}_{F_d} + \mathbf{h}_{FL}(t, \tilde{u}) \\ \Sigma_{2,FL} : \dot{\tilde{u}} &= \dot{u}^* - \gamma \mu(x, u^*, \tilde{u}) \left(-K_{FL} \mathbf{e} - \rho(u^* - \tilde{u}) \right) \end{aligned} \quad (38)$$

with

$$\begin{aligned} \boldsymbol{\xi}_{F_d} &= \mathbf{B}_{FL} \left(-\frac{\dot{\tilde{F}}_d}{M} + K_{FL} \begin{bmatrix} 0 \\ \tilde{F}_d \\ -\tilde{F}_d \\ M \end{bmatrix} \right) \\ \mathbf{h}_{FL}(t, \tilde{u}) &= -\mathbf{B}_{FL} \rho(\tilde{u}), \end{aligned} \quad (39)$$

and

$$\begin{aligned} \Sigma_{1,ST} : \dot{\boldsymbol{\vartheta}} &= f_{\boldsymbol{\vartheta}}(t, \boldsymbol{\vartheta}) + \mathbf{h}_{ST}(t, \tilde{u}) \\ \Sigma_{2,ST} : \dot{\tilde{u}} &= \dot{u}^* - \gamma \mu(x, u^*, \tilde{u}) \left(v^*(t, \boldsymbol{\vartheta}) - \rho(u^* - \tilde{u}) \right) \end{aligned} \quad (40)$$

with

$$\begin{aligned} f_{\boldsymbol{\vartheta}}(t, \boldsymbol{\vartheta}) &= \frac{\partial T}{\partial \zeta} \left\{ \frac{1}{|\zeta_1|} \begin{bmatrix} -\frac{k_1}{2} & 1 \\ -k_2 & 0 \end{bmatrix} T^{-1}(\boldsymbol{\vartheta}) - \begin{bmatrix} 0 \\ d \end{bmatrix} \right\} \\ \mathbf{h}_{ST}(t, \tilde{u}) &= -\frac{\partial T}{\partial \zeta} \begin{bmatrix} 1 \\ |\zeta_1| \\ 0 \end{bmatrix} \rho(\tilde{u} - \hat{u}) \end{aligned} \quad (41)$$

according to [22], where $v^*(t, \zeta)$ was defined in Eq. 25 and ζ corresponds to a coordinates transformation of the closed-loop dynamics. The detailed derivations are presented in Appendix.

Condition 4 coincides with the proof of stability of the controllers in their standard configuration, and is ensured by choosing the Lyapunov functions as:

$$\begin{aligned} V_{FL} &= \mathbf{e}^T P_{FL} \mathbf{e} \\ V_{ST} &= \boldsymbol{\vartheta}^T P_{ST} \boldsymbol{\vartheta}. \end{aligned} \quad (42)$$

Condition 5 is satisfied according to the result in [23], where it was proven that if $|\dot{u}^*| < \infty \forall t > 0$, then $\tilde{u}(t)$ is UUB for all time.

Finally, Condition 6 is verified as, $\Sigma_{1,FL}$:

$$\begin{aligned} \left\| \frac{\partial V_{FL}}{\partial \mathbf{e}} \mathbf{h}_{FL}(t, \tilde{u}) \right\| &\leq \|2P_{FL} \mathbf{e}\| \|B_{FL}\| |\rho(u^*) - \rho(u^* - \tilde{u})| \\ &\leq \|2P_{FL} \mathbf{e}\| \|B_{FL}\| L_p \|\tilde{u}\| \\ &\leq \underbrace{\|2P_{FL}\| \|B_{FL}\| L_p}_{\eta} \|\tilde{u}\|_{\infty} \|\mathbf{e}\|, \end{aligned} \quad (43)$$

and for $\Sigma_{1,ST}$,

$$\begin{aligned} \left\| \frac{\partial V_{ST}}{\partial \boldsymbol{\vartheta}} \mathbf{h}_{ST}(t, \tilde{u}) \right\| &\leq \|2P_{ST} \boldsymbol{\vartheta}\| \frac{L_p}{\min_t(|\zeta_1(t)|)} \|\tilde{u}\|_{\infty} \left\| \frac{\partial \tau}{\partial \boldsymbol{\xi}} \right\|_{\infty} \\ &\leq \underbrace{\|2P_{ST}\| \frac{L_p}{\min_t(|\zeta_1(t)|)} \|\tilde{u}\|_{\infty}}_{\eta'} \left\| \frac{\partial \tau}{\partial \boldsymbol{\xi}} \right\|_{\infty} \|\boldsymbol{\vartheta}\|. \end{aligned} \quad (44)$$

VI. CASE STUDY

The case study on which the algorithm is presented is a wind turbine pitch system with the hydraulic actuator used to provide a time-varying blade pitch, mainly according to prevailing wind and power demand. The mechanical link between cylinder and turbine blade is stiff, such that controlling the blade angle is equivalent to controlling cylinder position. The angular dynamics of the blade is described by:

$$\begin{aligned} J_{tot} \dot{v}_{\beta} &= (A_p p_p - A_r p_r) r \sin(\psi(x_c)) - M_{fric} - M_{ext} \\ \dot{\beta} &= v_{\beta}, \end{aligned} \quad (45)$$

where the equivalent mass M also accounts for blade inertia. It is noticed that the equations match the dynamics of the cylinder dynamics presented in Eq. 7. The presence of a cyclic component in the variable distance that relates mechanical moment to force is minor, as will be shown. Thus, the control design aims at tracking the angle while the cylinder dynamics represents a stable internal dynamics, under the assumption of having a stiff mechanical connection between cylinder and blade. Hence, there exists a static transformation relating x_c to β and with the pitch control error being the difference between pitch angle and a reference,

$$e = \beta - r, \quad (46)$$

the relative degree of the closed loop pitch control will be the same as for the closed loop cylinder piston position control loop analysed above. With relative degree three of both, the third derivative of the error is needed,

$$\begin{aligned} e^{(3)} &= -\frac{\dot{M}_{fric} + \dot{M}_{ext}}{J_{tot}} \\ &\quad - \frac{l A_p^2 B}{J_{tot} V_p} v_c \sin \psi_p(x_c) - \frac{l A_r^2 B}{J_{tot} V_r} v_c \sin \psi_p(x_c) \\ &\quad + \frac{l A_p B}{J_{tot} V_p} Q_p(u) \sin \psi_p(x_c) + \frac{l A_r B}{J_{tot} V_r} Q_r(u) \sin \psi_p(x_c) \\ &\quad + \underbrace{\frac{l}{J_{tot}} F_h \cos(\psi_p(x_c)) \frac{d\psi}{dx_c} v_c - r^{(3)}}_{\tau(x)} \triangleq \varpi. \end{aligned} \quad (48)$$

With respect to the general case presented in Eq. 8, two variations are present:

- $1/M$ is replaced by $l \sin \psi_p(x_c) / J_{tot}$.
- An additional term $\tau(x)$, is introduced.

These changes arise due to the variable-length moment arm in the updated dynamics.

However, Fig. 5 suggests that $\psi(x_c)$ is approximately constant, and thus the following assumptions are made:

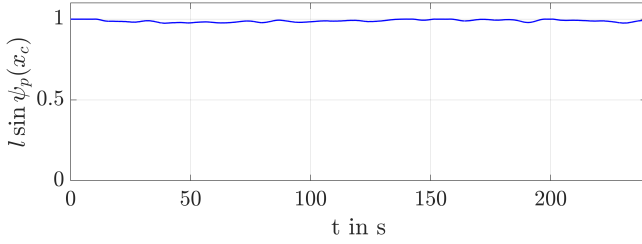


Fig. 5. Momentum arm angle for verifying that constant assumption holds.

- $\psi(x_c) \approx \text{const}$
- $\frac{d\psi}{dx_c} \approx 0 \rightarrow \tau(x) \approx 0$.

A. Standard controllers for study case

The control action for the standard cases are obtained by following the procedure described in Sec. III. The input gain is defined as

$$g = \frac{lA_p B}{J_{tot} V_p} K_{Qp} + \frac{lA_r B}{J_{tot} V_r} K_{Qr}. \quad (49)$$

The feedback linearization controller is derived as,

$$\begin{aligned} u_{FL} &= \frac{1}{g} \left[\frac{lA_p^2 B}{J_{tot} V_p} v_c + \frac{lA_r^2 B}{J_{tot} V_r} v_c + \frac{\dot{M}_d / J_{tot} + r^{(3)} - K_{FL} \mathbf{e}}{\sin(\psi_p(x_c))} \right], \\ &\approx \frac{1}{g} \left[\frac{lA_p^2 B}{J_{tot} V_p} v_c + \frac{lA_r^2 B}{J_{tot} V_r} v_c + \frac{\dot{M}_d}{J_{tot}} + r^{(3)} - K_{FL} \mathbf{e} \right], \end{aligned} \quad (50)$$

where the angle dependency is removed, since it only affects the $r^{(3)}$ term and the term associated with the gain, which is a degree of freedom anyway.

The same applies for the sliding mode controller:

$$\begin{aligned} u_{ST} &= \frac{1}{g} \left[\frac{\dot{M}_d}{J_{tot}} + \frac{lA_p^2 B}{J_{tot} V_p} v_c + \frac{lA_r^2 B}{J_{tot} V_r} v_c + r^{(3)} - \lambda_2 \ddot{\mathbf{e}} - \lambda_1 \dot{\mathbf{e}} \right. \\ &\quad \left. - k_1 [s]^{1/2} - k_2 \int_0^t \text{sgn}(s) d\tau \right], \end{aligned} \quad (51)$$

with

$$\begin{bmatrix} \dot{\mathbf{e}} \\ \ddot{\mathbf{e}} \end{bmatrix} \approx \begin{bmatrix} v_\beta - \dot{r} \\ -\frac{\dot{M}_d}{J_{tot}} + \frac{l(A_p p_p - A_r p_r)}{J_{tot}} - \ddot{r} \end{bmatrix} \quad (52)$$

and \hat{M}_d the new disturbance being estimated.

B. Mapping inversion based controllers for study case

Following the same approach, the virtual control input in the proposed solutions are:

$$v_{FL} = \frac{\dot{M}_d}{J_{tot}} + \frac{lA_p^2 B}{J_{tot} V_p} v_c + \frac{lA_r^2 B}{J_{tot} V_r} v_c + r^{(3)} - K_{FL} \mathbf{e} \quad (53)$$

$$\begin{aligned} v_{ST} &= \frac{\dot{M}_d}{J_{tot}} + \frac{lA_p^2 B}{J_{tot} V_p} v_c + \frac{lA_r^2 B}{J_{tot} V_r} v_c + r^{(3)} - \lambda_2 \ddot{\mathbf{e}} - \lambda_1 \dot{\mathbf{e}} \\ &\quad - k_1 [s]^{1/2} - k_2 \int_0^t \text{sgn}(s(\tau)) d\tau, \end{aligned} \quad (54)$$

and the dynamical mapping inversion algorithm is,

$$\begin{aligned} \dot{u} &= \gamma \mu(t, \mathbf{x}, u) (v - \rho(t, \mathbf{x}, u)) \\ \rho(t, \mathbf{x}, u) &= \frac{lA_p B}{J_{tot} V_p} Q_p(p_p, p_r, u) + \frac{lA_r B}{J_{tot} V_r} Q_{rv}(p_r, u) \\ \mu(t, \mathbf{x}, u) &= \frac{\partial K}{\partial u} \left(\frac{A_p B}{M V_p} \sqrt{\Delta_{pp}(u)} + \frac{A_r B}{M V_r} \sqrt{\Delta_{pr}(u)} \right), \end{aligned} \quad (55)$$

where $K(u)$ is defined according to Eq. 31 as

$$K(u) = 10^{-7} (-23.67u^5 + 40.73u^3 + 1.97u). \quad (56)$$

VII. SIMULATION RESULTS

The designed control actions are tested on a high-fidelity simulator, which includes the general dynamics presented in Eqs. 1,45, and also encompass the control valve dynamics. The measured signals are subjected to noise, simulated at realistic levels. The velocities (v_c and v_β) are obtained via numerical differentiation since they are not usually available as sensor signals in a real plant. The pitch angle reference and the disturbance M_{ext} are obtained from a high-fidelity simulator for a wind turbine based on OpenFAST that is widely used in wind turbine research and development.

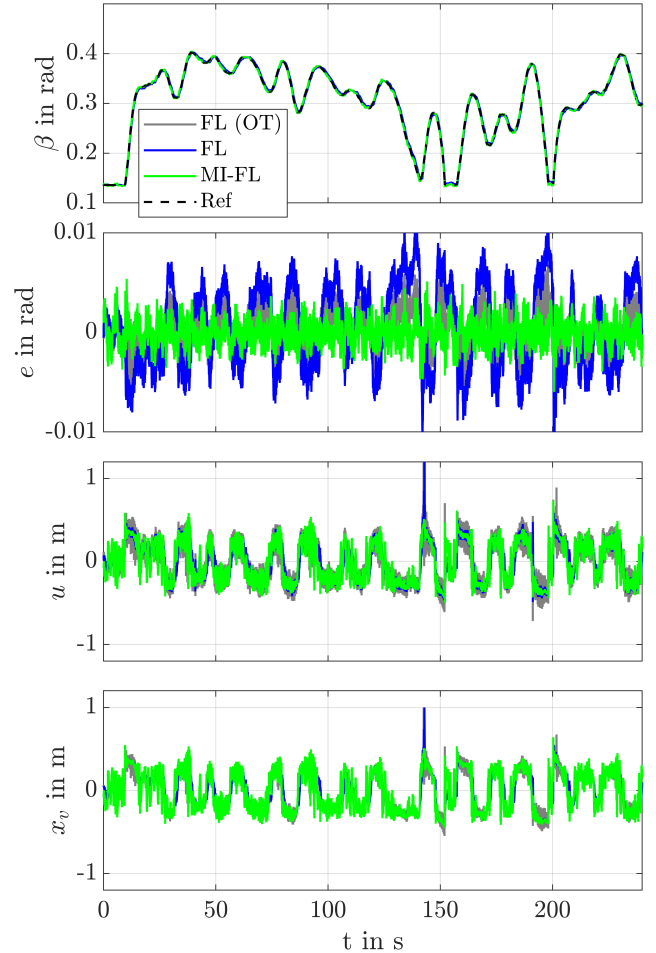


Fig. 6. Tracking performance of the Feedback linearization based controller, with and without applying the dynamical mapping inversion.

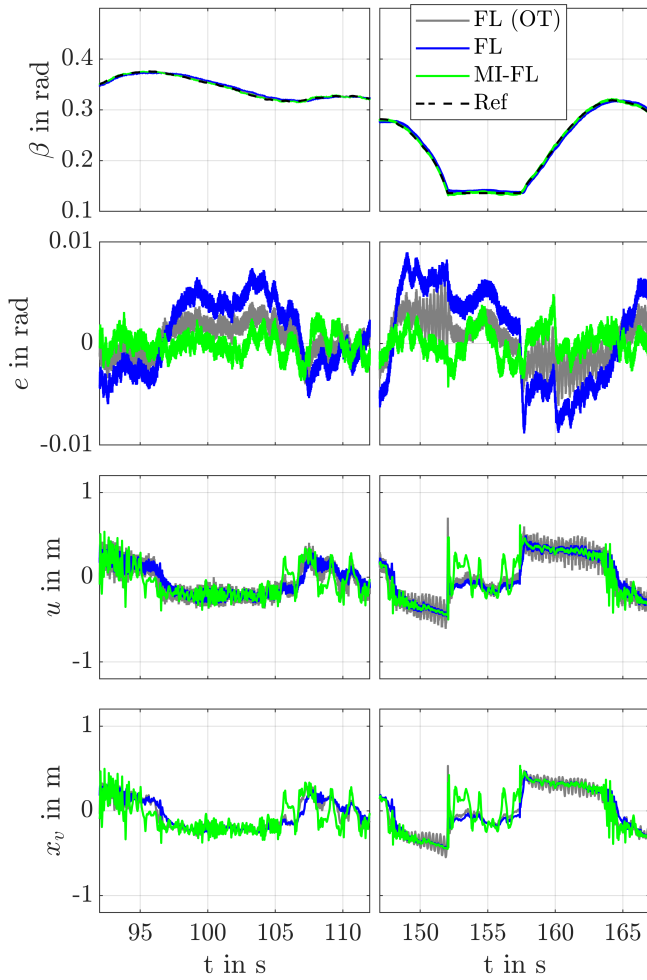


Fig. 7. Zoomed on regions of interest for showing the tracking properties under different conditions.

A. Tracking performance

The tracking performance of the feedback linearization controller is presented in Fig. 6, and in Fig. 7 in a zoomed version. Three controllers are presented, for comparing the standard Feedback Linearization (FL) solution with the one where the dynamic mapping inversion is applied (MI-FL) under the same tuning gains, and by overtuning (OT) the standard solution to be able to match the performance of the MI-FL controller. While both controllers are showing good tracking performance, the MI-FL (for a given tuning) shows a smaller error over the simulation window. By increasing the gains, it is possible to match its performance, with the consequence of getting an increase of unwanted chattering in the input.

The zoomed plot gives a visualization of the input behaviour u , and of the valve position x_v . The MI-FL controller shows a reduced chatter in the regions where the pitch is varying in amplitude, while it shows a more chattering behaviour when the pitch is constant or slowly varying. Furthermore, the signal quality in u and x_v are equivalent for the MI solution, while part of the noise is filtered out by the valve dynamics in the standard solution, since the controller doesn't have knowledge

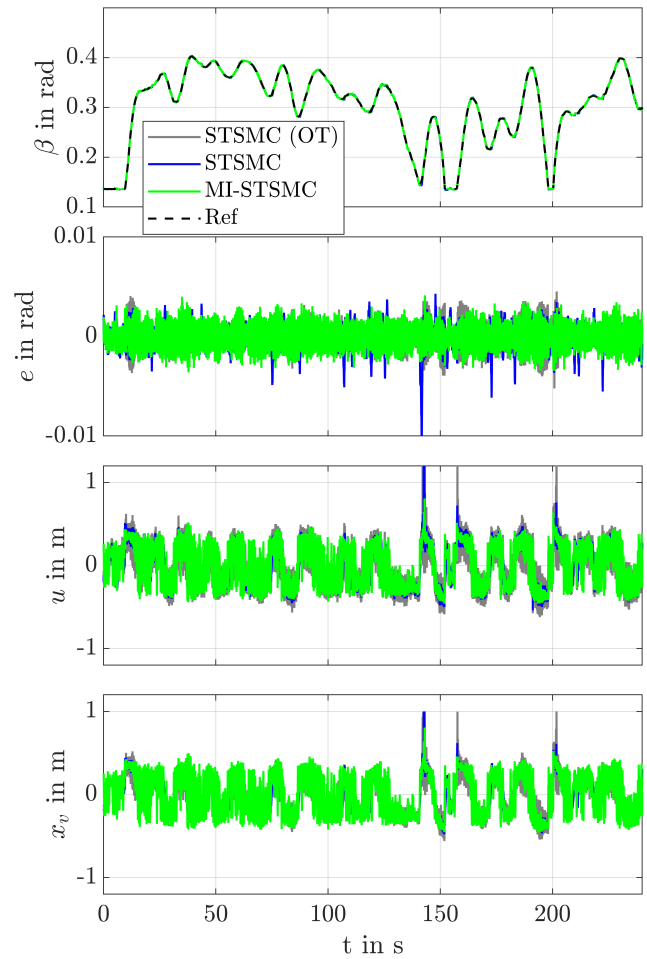


Fig. 8. Tracking performance of the Supertwisting sliding mode controllers, with and without applying dynamical mapping inversion.

of the valve dynamics, nor of valve limitations.

The results for the ST-SMC are stated in Fig. 8.

The tracking performances are more similar between the two solutions with respect to the FL controller. The OT version doesn't improve the tracking performance although leading to a more chattering input. The disturbance rate that the controller needs to handle, is shown in Fig. 9, where it is evident how higher gains lead to a larger amplitude in the command signal.

The unexpected dependency of the disturbance rate on the tuning gains is justified by the use of an observer for estimating the disturbance. Higher gains lead to a higher error in the estimation, which is affecting the overall control performance. The performance comparison of the observer with the different controllers is stated in Fig. 10. The tuning doesn't coincide with the bounds since higher gains are reflected with higher disturbance estimation errors and, thus, higher disturbance derivative bounds. The STSMC is not capable of ensuring convergence on the origin at any time instant, but boundedness is guaranteed, according to [24].

B. Mapping inversion algorithm

The tracking performance of the mapping inversion algorithm is presented in Fig. 11. v and ρ are the signal defined in

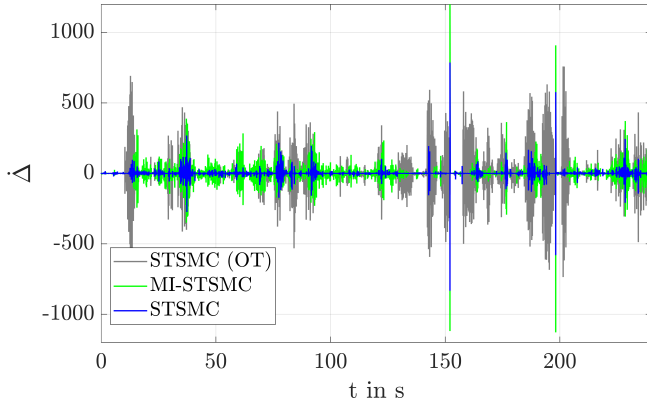


Fig. 9. Perturbation derivative of sliding mode dynamics under different STSMC.

Eq. 55, while v_{sim} is the equivalent of the v signal which is obtained in simulation, hence based on the real states of the system and not on the noisy measurements. The algorithm is not able to perfectly reconstruct v , because of the presence of noise in the signals. However, it is shown how it is possible to determine a proper tuning such that it is possible to reconstruct the actual virtual input in the plant (v_{sim}) and filtering out the noise present in the measurements.

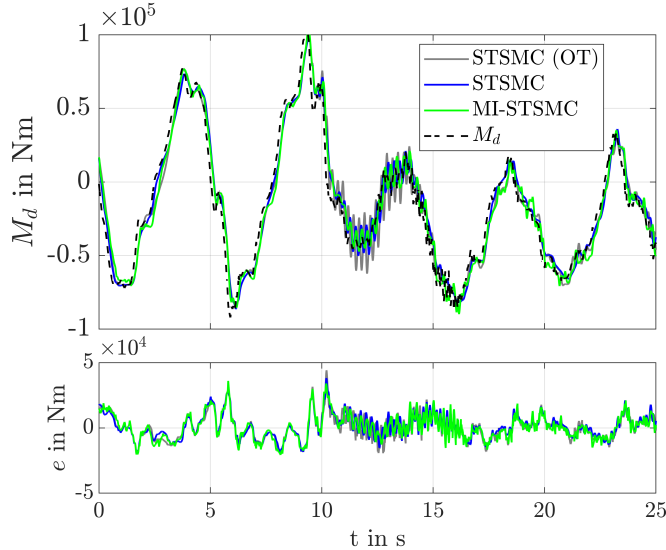


Fig. 10. Wind load disturbance estimation and comparison with LPF hydraulic force.

Thus, there is a natural filtering action which can be approximate with a simple first order low-pass filter in order to determine an indication of the bandwidth of such filtering action, in comparison to the bandwidth of the valve which represents a physical limitation in what the control action can deliver on the real system. The comparison is presented in Fig. 12.

The cutoff frequency of the MI algorithm is lower than the valve's bandwidth, meaning the valve only needs to follow trajectories it can actually withstand. With respect to the standard solution, where the filtering was occurring in the

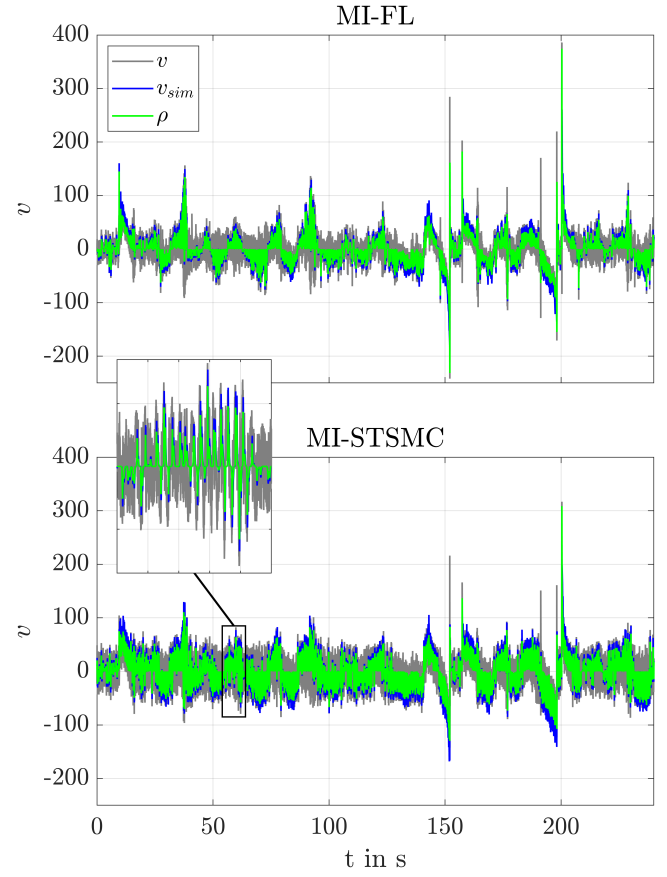


Fig. 11. Dynamical mapping inversion algorithm capability of tracking the required virtual controller, with a filtering action that allows to reconstruct the actual signal value in simulation

valve directly, in this new solution is the algorithm accounting for the valve limitations and filtering the input signal. This result support the similar signal quality in u and x_v in the MI solution that was found in Fig. 7.

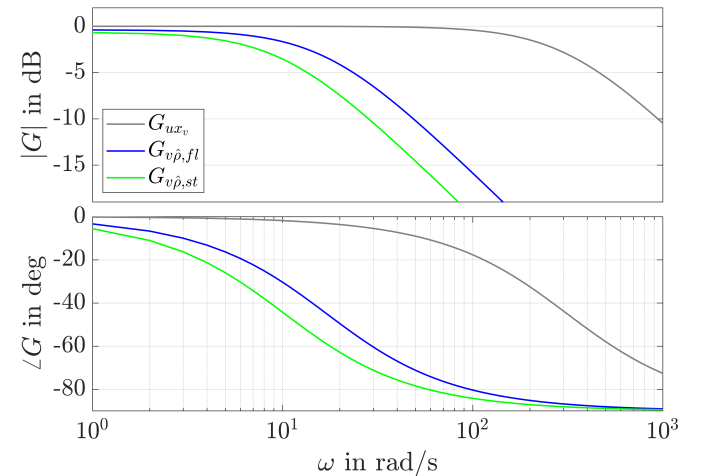


Fig. 12. Bode plots of valve dynamics and mapping inversion filtering effect.

Remark 3. The tuning presented shows some room with

respect to the maximum bandwidth that can be achieved by the valve. However, a faster tuning is reflected in a noisier reconstruction of v_{sim} from the noisy measurements, hence more chattery u and x_v . The slew rate limitation of the valve may also play a role.

C. Controllers comparison

While the plots are able to display some clear properties of the system and some qualitative performance indications can be obtained from them, a more rigorous analysis is performed to have a quantitative description and comparison of the proposed solutions. The controllers are tested according to some metrics, related both to the tracking performance and to the input cleanliness.

Assessing the tracking performance based on the error is straightforward, while assessing the signal quality of the input is more challenging since it is not a constant average signal. The solution was to calculate a moving average \bar{u} and defining a new signal $u_f = u - \bar{u}$ which has zero mean and still maintains the information of the high frequency oscillation. The moving average window is the same for all the tests. The same applies for determining $x_{v,f}$. An example of a u_f signal is illustrated in Fig. 13.

The following metrics are defined for the purpose:

- $RMS(u_f) = \sqrt{\frac{1}{N} \sum_{i=1}^N u_{f,i}^2}$
- $RMS(x_{v,f}) = \sqrt{\frac{1}{N} \sum_{i=1}^N x_{v,f,i}^2}$
- $MAX(e) = \max_{0 \leq t \leq T} e(t)$
- $RMS(e) = \sqrt{\frac{1}{N} \sum_{i=1}^N e_i^2}$
- $QWAE(e) = \sqrt{\frac{\sum_{i=1}^N |e_i|}{\sum_{i=1}^N e_i^2}}$
- $ISE(e) = \int_0^T e^2(t) dt$

where T is the simulation time and the resulting values are normalized for having a clearer comparison. The QWAE

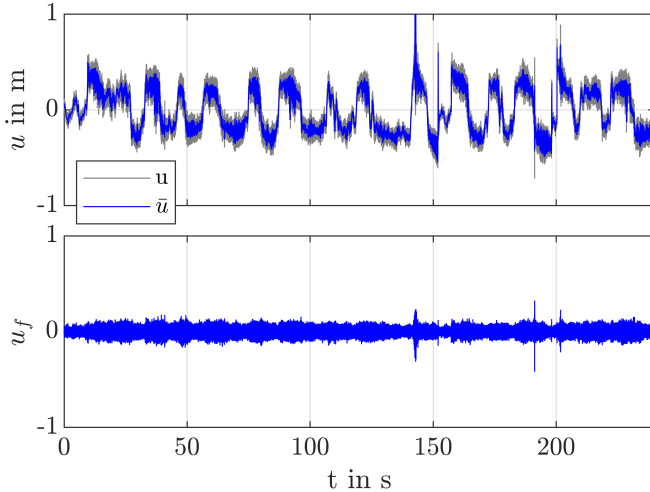


Fig. 13. Moving average removal for deriving a metrics associated with signal chatter.

(Quadratically Weighted Average Error) metric is used to penalize larger errors more heavily, while the ISE (Integral Squared Error) metric measures the persistence of errors.

The result for the system running with the different controllers is shown in Fig. 14.

The solution proposed in the article performs better than standard one with the same tuning and with higher gains. The only exceptions are the cases of the $RMS(e)$ and the $ISE(e)$, where the OT ST-SMC displays a slightly smaller error, at the price of having much worse input performance. For a fixed tuning, the error with the MI is lower than when applying the respective standard algorithm.

The input signal is significantly improved by the filtering action of the MI, while the improvement in the actual valve position becomes less significant thanks to the filtering action of the valve itself. Still, the solution that leverages the MI shows the cleanest input over a window where both fast varying and constant references are required. The amplitude of $RMS(u_f)$ and $RMS(x_{v,f})$ are equivalent in the MI case.

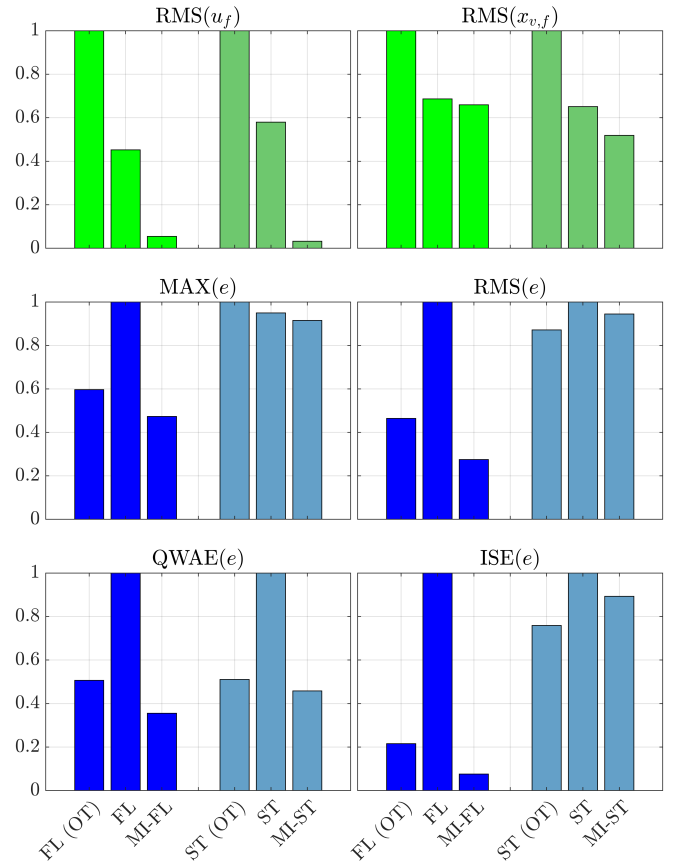


Fig. 14. Bar plots for evaluating performance of the different controllers according to different metrics, associated with control input and tracking error.

VIII. CONCLUSION

This article presented a solution to eliminate the formation of an algebraic loop when designing some conventional non-linear controllers. This was achieved by design of a virtual input and dynamically deriving a control action, which emulated the desired behaviour, while control valve trajectory commands were avoided if they would exceed the specified admissible range for valve behaviours.

The effectiveness of the proposed solution was tested in high-fidelity simulation for the industrial application of wind

turbines' blade pitch control, showing a general improvement in tracking performance and an essential reduction of input chatter, especially in the regions where the pitch reference is highly varying.

The dynamic inversion solution enabled room for flexibility and allows for future progress with other nonlinear parameter estimation algorithms.

A further step towards industrial implementation will be to derive the discrete-time version of the algorithm.

ACKNOWLEDGEMENTS

This research was funded by The Danish Energy Technology Development and Demonstration Programm (EUDP) through the project: "Decreased Cost of Energy (CoE) from wind turbines by reducing pitch system faults", grant number 64022-1058. The authors much appreciate this support.

APPENDIX

FEEDBACK INTERCONNECTED SYSTEMS DERIVATIONS

Let $\delta_{\mathbf{e}}$ be the error associated with the calculation of \ddot{e} . The closed-loop system with the FL controller in the form of Σ_{FL} is obtained as:

$$\begin{aligned} \dot{\mathbf{e}} &= \mathbf{A}_{FL}\mathbf{e} + \mathbf{B}_{FL}(v^* - \tilde{v}) \\ &= \mathbf{A}_{FL}\mathbf{e} + \mathbf{B}_{FL} \left(-K_{FL}(\mathbf{e} - \delta_{\mathbf{e}}) - \frac{\dot{\tilde{F}}_d}{M} - \tilde{v} \right) \\ &= (\mathbf{A}_{FL} - \mathbf{B}_{FL}K_{fl})\mathbf{e} + \mathbf{B}_{FL} \left(K_{FL} \begin{bmatrix} 0 \\ -\frac{\dot{\tilde{F}}_d}{M} \end{bmatrix} - \frac{\dot{\tilde{F}}_d}{M} \right) \\ &\quad - \mathbf{B}_{FL} [\rho(\tilde{u}) - \rho(u^* - \tilde{u})] \\ &= (\mathbf{A}_{FL} - \mathbf{B}_{FL}K_{fl})\mathbf{e} + \boldsymbol{\xi}_{F_d} + \mathbf{h}_{FL}(t, \tilde{u}). \end{aligned} \quad (57)$$

The unperturbed system is $\mathbf{h}_{FL}(t, 0) = \mathbf{0}$ and the remaining terms describe the closed-loop dynamics with the standard design. Except for the bounded term $\boldsymbol{\xi}_{F_d}$, the system is exponentially stable with a convergence rate determined by the eigenvalues of $\mathbf{A}_{FL} - \mathbf{B}_{FL}K_{fl}$. The bounded term acts as a disturbance that causes the system to be UUGB with sufficiently high gains.

Let

$$\tilde{s} = s - s^*, \quad (58)$$

where s is the actual value of the sliding variable and s^* is calculated by differentiating the error with a robust exact differentiator, like the one in [25]. The sliding variable dynamics in closed loop reads:

$$\begin{aligned} \dot{s} &= -k_1 |s^*|^{1/2} - k_2 \int_0^t \text{sgn}(s^*(\tau)) d\tau \\ &\quad - k_1 |\tilde{s}|^{1/2} - k_2 \int_0^t \text{sgn}(\tilde{s}(\tau)) d\tau - \frac{\dot{\tilde{F}}_d}{M} - \lambda_2 \frac{\tilde{F}_d}{M} \\ &\quad - \rho(u^* - \tilde{u}) \\ &= -k_1 |s^*|^{1/2} - k_2 \int_0^t \text{sgn}(s^*(\tau)) d\tau - \Delta(t) - \rho(u^* - \tilde{u}), \end{aligned} \quad (59)$$

where all the terms in Δ are bounded: \tilde{s} is bounded and with zero mean, since the reconstruction error with the robust exact differentiator is only related to noise, and the disturbance estimations are bounded (proof in Sec. III-C1). For $s \neq 0$ one can define [22]

$$\begin{aligned} \zeta_1 &\triangleq |s^*|^{1/2} \text{sgn}(s^*) \\ \zeta_2 &\triangleq -k_2 \int_0^t \text{sgn}(s^*(\tau)) d\tau - \Delta(t) \\ \boldsymbol{\zeta} &\triangleq [\zeta_1 \quad \zeta_2]^T, \end{aligned} \quad (60)$$

and rewrite the closed-loop system as:

$$\dot{\boldsymbol{\zeta}} = \frac{1}{|\zeta_1|} \begin{bmatrix} -\frac{1}{2}k_1 & 1 \\ -k_2 & 0 \end{bmatrix} \boldsymbol{\zeta} + \begin{bmatrix} 0 \\ -d \end{bmatrix} + \underbrace{\begin{bmatrix} -\frac{\rho(u - \tilde{u})}{|\zeta_1|} \\ 0 \end{bmatrix}}_{\mathbf{h}(t, \tilde{u})}, \quad (61)$$

with k_1, k_2 selected to fulfil the conditions in [26]. Since $\mathbf{h}(t, 0) = 0$, the unperturbed system has a finite stable equilibrium point at the origin. This implies (see [22]) the existence of a diffeomorphism $T : \mathbb{R}^2 \rightarrow \mathbb{R}^2$ such that for $\boldsymbol{\vartheta} = T(\boldsymbol{\zeta})$ and

$$\begin{aligned} \dot{\boldsymbol{\vartheta}} &= \frac{\partial T}{\partial \boldsymbol{\zeta}} \left\{ \frac{1}{|\zeta_1|} \begin{bmatrix} -\frac{k_1}{2} & 1 \\ -k_2 & 0 \end{bmatrix} T^{-1}(\boldsymbol{\vartheta}) - \begin{bmatrix} 0 \\ d \end{bmatrix} \right\} - \frac{\partial T}{\partial \boldsymbol{\zeta}} \begin{bmatrix} 1 \\ |\zeta_1| \\ 0 \end{bmatrix} \rho(\tilde{u} - \hat{u}), \\ \exists V_{ST} &= \boldsymbol{\vartheta}^T P_{ST} \boldsymbol{\vartheta} \text{ such that } V_2 \leq -c \|\boldsymbol{\vartheta}\| \triangleq -W_{ST}(\|\boldsymbol{\vartheta}\|). \end{aligned} \quad (62)$$

REFERENCES

- [1] T. Fossen, *Marine Control Systems: Guidance, Navigation and Control of Ships, Rigs and Underwater Vehicles*, Dec. 2002, vol. 28.
- [2] J. Walgern, K. Fischer, P. Hentschel, and A. Kolios, "Reliability of electrical and hydraulic pitch systems in wind turbines based on field-data analysis," *Energy Reports*, vol. 9, pp. 3273–3281, Dec. 2023.
- [3] A. Dallabona, M. Blanke, H. C. Pedersen, and D. Papageorgiou, "Fault diagnosis and prognosis capabilities for wind turbine hydraulic pitch systems," *Mechanical Systems and Signal Processing*, vol. 224, p. 111941, Jan. 2025.
- [4] B. Ayalew and B. Kulakowski, "Cascade tuning for nonlinear position control of an electrohydraulic actuator," in *2006 American Control Conference*. Minneapolis, MN, USA: IEEE, 2006, p. 6 pp.
- [5] A. Dallabona, M. Blanke, and D. Papageorgiou, "Friction Estimation for Condition Monitoring of Wind Turbine Hydraulic Pitch System," *IFAC-PapersOnLine*, vol. 58, no. 4, pp. 598–603, 2024.
- [6] S. Koch and M. Reichhartinger, "Observer-based sliding mode control of hydraulic cylinders in the presence of unknown load forces," *e & i Elektrotechnik und Informationstechnik*, vol. 133, no. 6, pp. 253–260, Sep. 2016.
- [7] A. T. Thomas, R. Parameshwaran, S. Sathiyavathi, and A. V. Starbino, "Practical profile tracking for a hydraulic press using sliding mode controller," *Proceedings of the Institution of Mechanical Engineers, Part C: Journal of Mechanical Engineering Science*, vol. 236, no. 2, pp. 1202–1213, Jan. 2022.
- [8] C. Guan and S. Pan, "Adaptive sliding mode control of electro-hydraulic system with nonlinear unknown parameters," *Control Engineering Practice*, vol. 16, no. 11, pp. 1275–1284, Nov. 2008.
- [9] J. Komsta, N. van Oijen, and P. Antoszkievicz, "Integral sliding mode compensator for load pressure control of die-cushion cylinder drive," *Control Engineering Practice*, vol. 21, no. 5, pp. 708–718, May 2013.
- [10] M. A. Estrada, M. Ruderman, and L. Fridman, "Super-twisting based sliding mode control of hydraulic actuator without velocity state," *Control Engineering Practice*, vol. 142, p. 105739, Jan. 2024.
- [11] Cheng Guan and Shuangxia Pan, "Nonlinear Adaptive Robust Control of Single-Rod Electro-Hydraulic Actuator With Unknown Nonlinear Parameters," *IEEE Transactions on Control Systems Technology*, vol. 16, no. 3, pp. 434–445, May 2008.

- [12] M. Choux, G. Hovland, and M. Blanke, "Cascade Controller Including Backstepping for Hydraulic-Mechanical Systems," *IFAC Proceedings Volumes*, vol. 45, no. 8, pp. 310–315, Jan. 2012.
- [13] F. Bakhshande and D. Söffker, "Proportional-Integral-Observer-Based Backstepping Approach for Position Control of a Hydraulic Differential Cylinder System With Model Uncertainties and Disturbances," *Journal of Dynamic Systems, Measurement, and Control*, vol. 140, no. 12, p. 121006, Dec. 2018.
- [14] I. Manganas, L. Schmidt, T. O. Andersen, and H. C. Pedersen, "Backstepping based controller utilizing a sliding mode disturbance observer," *Modeling, Identification and Control: A Norwegian Research Bulletin*, vol. 44, no. 1, pp. 31–42, 2023.
- [15] M. Choux and G. Hovland, "Adaptive Backstepping Control of Nonlinear Hydraulic-Mechanical System Including Valve Dynamics," *Modeling, Identification and Control: A Norwegian Research Bulletin*, vol. 31, no. 1, pp. 35–44, 2010.
- [16] H. F. Grip, T. A. Johansen, L. Imsland, and G.-O. Kaasa, "Parameter estimation and compensation in systems with nonlinearly parameterized perturbations," *Automatica*, vol. 46, no. 1, pp. 19–28, Jan. 2010.
- [17] D. Papageorgiou, M. Blanke, H. H. Niemann, and J. H. Richter, "Robust Backlash Estimation for Industrial Drive-Train Systems—Theory and Validation," *IEEE Transactions on Control Systems Technology*, vol. 27, no. 5, pp. 1847–1861, Sep. 2019.
- [18] F. Bakhshande and D. Soffker, "Robust control approach for a hydraulic differential cylinder system using a Proportional-Integral-Observer-based backstepping control," in *2017 American Control Conference (ACC)*. Seattle, WA, USA: IEEE, May 2017, pp. 3102–3107.
- [19] Y. Shtessel, C. Edwards, L. Fridman, and A. Levant, *Sliding Mode Control and Observation*, ser. Control Engineering. New York, NY: Springer, 2014.
- [20] F. Bordry and A. Bruciapaglia, "An Augmented Observer for Measurement in a Deterministic Disturbed Environment - An Application in Control," in *Components and Instruments for Distributed Control Systems*. Elsevier, 1983, pp. 105–108.
- [21] A. Loria, "From feedback to cascade-interconnected systems: Breaking the loop," in *2008 47th IEEE Conference on Decision and Control*. Cancun, Mexico: IEEE, 2008, pp. 4109–4114.
- [22] J. A. Moreno and M. Osorio, "Strict Lyapunov Functions for the Super-Twisting Algorithm," *IEEE Transactions on Automatic Control*, vol. 57, no. 4, pp. 1035–1040, Apr. 2012.
- [23] D. Papageorgiou, M. Blanke, H. Henrik Niemann, and J. H. Richter, "Backlash estimation for industrial drive-train systems," *IFAC-PapersOnLine*, vol. 50, no. 1, pp. 3281–3286, Jul. 2017.
- [24] D. Papageorgiou and C. Edwards, "On the behaviour of under-tuned super-twisting sliding mode control loops," *Automatica*, vol. 135, p. 109983, Jan. 2022.
- [25] A. Levant, "Higher-order sliding modes, differentiation and output-feedback control," *International Journal of Control*, vol. 76, no. 9-10, pp. 924–941, Jan. 2003.
- [26] A. Chalanga and F. Plestan, "Finite Time Stabilization of An Uncertain Chain of Integrators by Integral Sliding Mode Approach," *IFAC-PapersOnLine*, vol. 50, no. 1, pp. 9613–9618, Jul. 2017.